AUTOMATING SEA ICE CHARACTERISATION FROM X-BAND SAR WITH CO-LOCATED AIRBORNE LASER SCANNER DATA OBTAINED DURING THE MOSAIC EXPEDITION

Karl Kortum[1,2]*, Suman Singha*[1]*, Gunnar Spreen*[2]*, Stefan Hendricks*[3]

[1]Remote Sensing Technology Institute (IMF), German Aerospace Center (DLR), Bremen, Germany,
[2] Institute of Environmental Physics, University of Bremen, Bremen, Germany,
[3] Alfred Wegener Institute for Polar and Marine Research, Bemerhaven, Germany

ABSTRACT

The research vessel 'Polarstern', moored to an ice floe, completed a year long drift with Arctic pack ice in the autumn of 2020. During that expedition, named MOSAiC, a comprehensive data set of airborne laser scanner (ALS) and spaceborne X-band SAR images in the area of the research vessel was acquired. With successful fusion of these two measurements, we can extrapolate sea ice features from the ALS data to the entire SAR scene using a convolutional neural network (CNN). From two preliminary scenes of ALS data we are able to show this for classes of sea ice roughness. This will be the basis for more comprehensive research, once the complete data set is available.

Index Terms— Sea Ice, SAR, ALS, CNN

1. INTRODUCTION

Supervised sea ice classification and characterisation from synthetic aperture radar imagery (SAR) is to this day heavily reliant on manual ice charting (eg. [1], [2])) and thus subject to human interpretation, errors and bias. Unsupervised approaches on the other hand use largely segmentation techniques, where the predicted classes then have to be manually mapped to some physical classes (eg. [3]). Until now it was not possible to overcome this human interaction with the data, since there was no comprehensive ground truth data available year round (satellite altimeters in principle could be used, as their accuracy is competitive [4], however this has not been investigated - probably due to the lack of 2D capability). In the advent of the MOSAiC mission, however, this has changed. We will soon have access to these types of data sets and be able to train more comprehensive models accordingly. ALS Data has in the past been shown to relate to ice classes significantly [5]. We initially analyse two ALS scenes to develop and test the methods to then be used on the entirety of the fully processed data, once it is available.

Data used in this manuscript was produced as part of the international Multidisciplinary drifting Observatory for the Study of the Arctic Climate (MOSAiC) with the tag MOSAiC20192020. Thanks also to DFG Projekt 'MOSAiCmicrowaveRS' for funding.

2. MEASUREMENTS

The elevation measurements used for this research comprise of two ALS scenes. One is from the 24th of December 2019, between 07:40:00 to 09:16:33 UTC, the other from the 25th of December, collected between 14:07:53 and 15:40:25 UTC. The ALS data has been acquired by a a helicopter flying a mow-the-lawn pattern over the MOSAiC floe. The resulting scenes have a geospatial resolution (grid spacing) of 0.5 meters. The two TerraSar-X dualpol stripmap scenes used were acquired around 00:49:46 UTC on the 24th and around 06:50:40 UTC on the 25th of December 2019. These have a pixel spacing of 6.6 meters. It should also be noted that at an incidence angle of $55°$, these images are taken outside of full performance range. In this time frame (2019-12-24-07:40:00 to 2019-12-25-15:40:00 UTC) The Polarstern had drifted from $113.49°$ lon, $86.63°$ lat to $115.12°$ lon, $86.63°$ lat.

Here we use the rapid release ALS data that has been produced during the campaign without the final and precise inertial processing of the INS/GPS data. Thus the data includes uncertainties in the surface elevations manifesting in elevation gradients. These gradients are apparent to be non-physical as they do not match up at intersecting segments. An example of this can be seen in (Fig. 1). Also some inaccuracies seen as periodic surface undulations can be observed particular at the edges of measurement segments. These were masked out by considering only the centre of segments. Some additional filtering was performed manually to combat these artefacts.

3. PRODUCT MATCHING

The ALS and SAR scenes to be matched have not been acquired at the same time. Thus, due to drift, simple geolocation is not enough to obtain reasonable matching of products. To overcome this, both measurements are converted into MOSAiCs local FloeNavi Coordinate System (Fig. 2). Now the different measurements can be matched. However, one should note, that this assumes the driftfield to be spatially invariant in the entire area by extrapolating the Polarstern drift

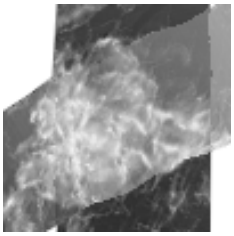

(a) Elevation measurement

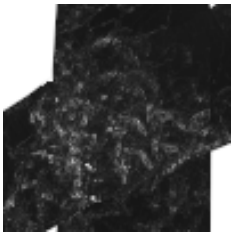

(b) Extracted std. deviation

Fig. 1. Example of ALS artefacts of incomplete processing (a) and how local standard deviation is mostly unaffected by these effects (b)

vector to a constant drift field. This means that drift correction is applied equally for each point at a given time and so real relative motion of the surrounding ice can not be corrected for and is a potential cause of error.

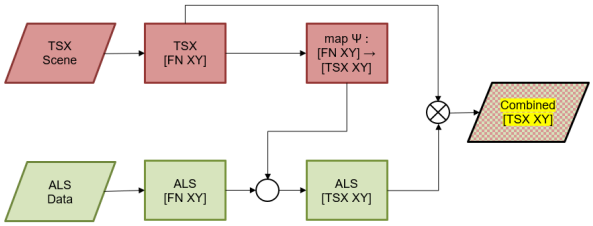

Fig. 2. Flowchart for the matching of ALS and TerraSar-X (TS-X) data. Coordinate systems are TSX pixel coordinates [TSX] and FloeNavi coordinates [FNXY]

The process of matching starts by converting both measurements geographic coordinates to MOSAiCs internal coordinate system, named FloeNavi coordinates. A map is computed, which maps from FloeNavi coordinates to the satellite scenes pixel coordinates. It is used to convert the ALS coordinates to satellite pixel coordinates. Now every point of ALS data has an assigned pixel coordinate of the satellite product. As the ALS data has a significantly higher resolution, multiple ALS data points will be mapped to the same TS-X pixel. For an illustration of the quality of matching, the mean over all ALS points pertaining to the same pixel is computed (Fig. 3). For a roughness estimate the standard deviation is used (Fig. 1), as in [6].

4. EXTRACTION OF LABELS

The actual ALS measurements itself are not used as ground truth for the CNN model - this would be very difficult with the artefacts in the measurements discussed in (sec. 2). Instead, the standard deviation of all ALS data points mapped to the same SAR pixel is computed to obtain a surface roughness. To derive labels the std. deviation is split into three

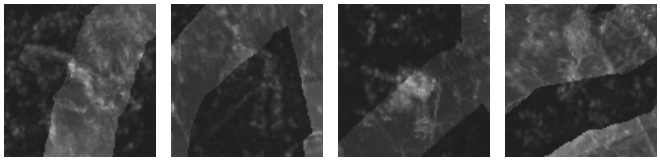

Fig. 3. Examples of quality of matching. Brighter strips are from the ALS measurements, darker backgrounds are the satellite products' backscatters.

classes of roughness, which makes it easier to gauge the models performance visually and relates more closely to the ice classification that is planned in the future. The probability density function (PDF) of the deviations (Fig. 4) has no apparent splits. One thresholds used for classification is chosen to be near the inflection point of the PDF peak, as an estimate for level ice. The deformed ice class threshold is chosen so that manually discerned frozen over leads fall entirely into this class and make no contribution to the heavily deformed ice. The classes are defined as seen in (Table 1).

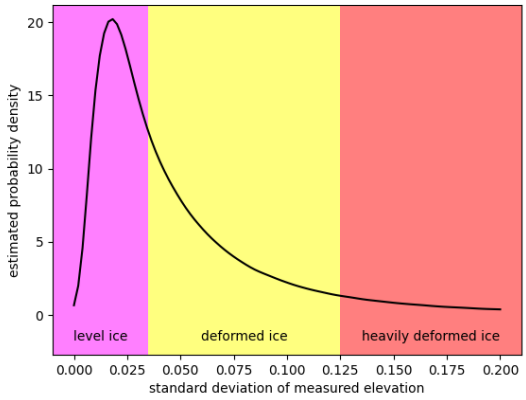

Fig. 4. Estimated probability density function (PDF) for all standard deviations measured. Ice classes are colour coded as per (Table 1).

Initialization	name	std. dev. σ [cm]	colour
LI	level ice	$\sigma < 3.5$	magenta
FI	deformed ice	$3.5 < \sigma < 12.5$	yellow
HDI	heavily deformed ice	$12.5 < \sigma$	red

Table 1. Table of class definitions for data labels used as ground truth to train the model.

The classes were also smoothed with a small Gaussian filter for more meaningful spatial separation of classes. The classes generated from the flight on the 24th are shown in (Fig 5).

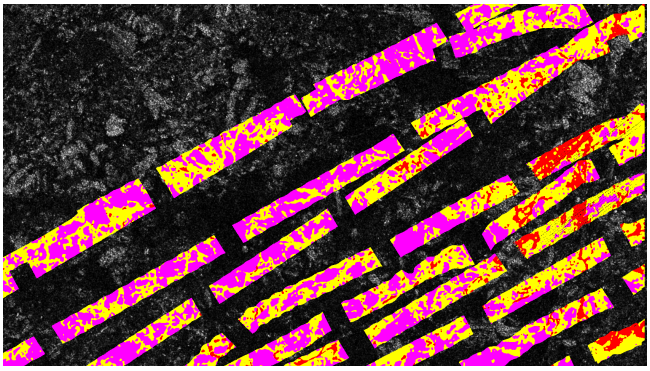

Fig. 5. Classes generated from the ALS scene on the 24th of December. The background is the HH backscatter from the corresponding satellite scene. Class definitions can be seen in (Table 1).

5. CLASSIFICATION

The model used for classification is a deep convolutional network built and trained in tensorflow, which is fed with four inputs for every pixel to be classified.

(1) The surrounding 7×7 pixel patch of the full resolution TS-X scene in four channels (HH, VV, HH/VV, HH-VV), normalised using a $\tanh$ function and then stretched to the value range $[0, 255]$.
(2) The surrounding 32×32 pixel patch of the TS-X scene down-sampled by a factor of 7 (full resolution patch size) in four channels (HH, VV, HH/VV, HH-VV), normalised using a $\tanh$ function and then stretched to the value range $[0, 255]$.
(3) The entire scene resized to 64×64 pixels, normalised using a $\tanh$ function.
(4) List of incidence angle and the stretching factors of inputs 1. and 2. (minimums and maximums of those patches).

A plot of the network's graph can be seen in (Fig 6). The polarisation features HH/VV and HH-VV were chosen, as they have shown promise for ice type classification in the past [7]. As 2D convolutional layers cannot learn these inter-layer operations, it seems prudent to include them manually.

The data is randomly split into mutually exclusive training and validation sets of 1300000 and 20000 samples respectively. The model achieves 61.5% accuracy on training and 59% accuracy on validation data. The results per class on unseen validation data are shown in a table below (Table 2). We want to note here, that we also attempted to train a VGG-16 style architecture with 32x32 patches as input, but this network failed to converge to a solution, not surmounting .33 accuracy in training.
A discrete classification of the entire scene from the 24th of December is is shown below (Fig. 7).

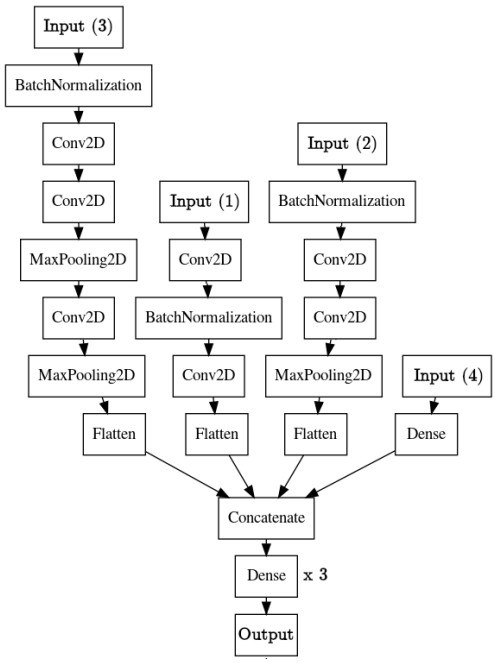

Fig. 6. Plot of the CNN model used for classification. See 5 for input definitions

	LI	DI	HDI
LI	64.01%	26.60%	9.39%
DI	27.72%	39.23%	33.05%
HDI	5.31%	23.95%	70.75%

Table 2. Table showing the percentage of networks' predicted classes (cols) for all ground truth labels (rows) on unseen data. For example 26.6% of data points of level ice (LI) were incorrectly predicted to be deformed ice (DI).

6. DISCUSSION

The results of the classifier are not ground breaking purely from a numerical standpoint. However, there are some aspects that need to be considered when drawing conclusions from our models performance. First of all SAR imagery's object resolution is not as big as pixel resolution. Secondly, next to surface roughness, volume scattering plays a significant role to radar response as well. This however, is not reflected in the training labels and is impossible to gauge from contextual data. Thus, we expect the model to perform better in regions were volume scattering is suppressed, such as lossy mediums like young ice with higher salinity and low freeboard, or in strongly deformed regions, where surface backscatter dominates. Finally, the elevation deviation domains have no meaningful separation in (Fig. 4). Thus we need to expect some mixing between those classes to occur naturally, especially in the deformed ice class (class ii).
Looking at the table of results (Table 2), our expectations

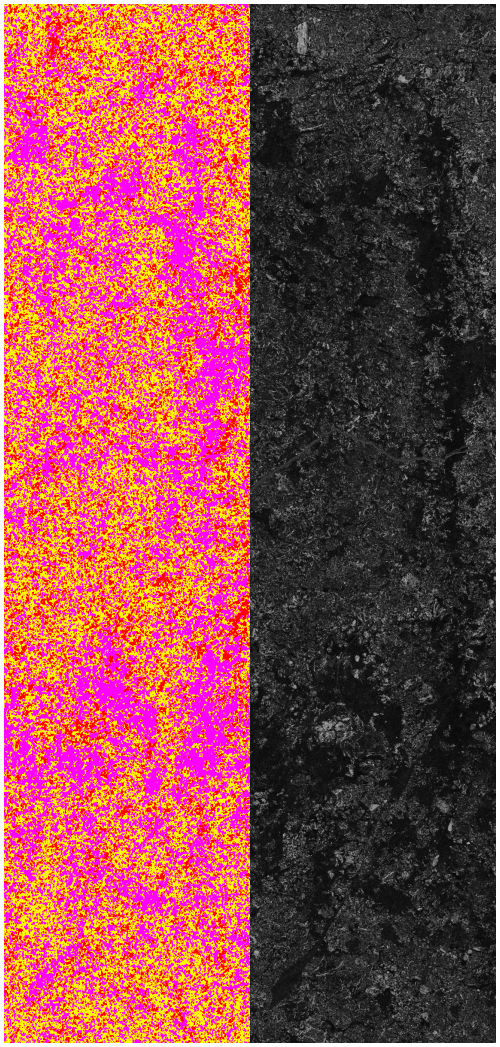

Fig. 7. Classified satellite scene from the 24th of December. Class definitions can be seen in (Table 1). The right hand side shows the HH backscatter.

come to fruition rather accurately. We see meaningful separation between rough and smooth ice, whilst separation from the deformed ice class (ii) proves difficult. This is underlined by (Fig. 7), where smooth magenta regions are well identified and correspond to dark regions in the satellite scenes. The speckling of other classes of these regions is probably due to ridges and deformations that are not easily visible in the satellite image, but are discernible from the ALS data used for training (Fig. 5).

7. CONCLUSION

The reasons for the models shortcomings in some regions can be well explained by physical features of the ice and the nature of these measurements. The success in separation between some of these classes and consistent extrapolation to unseen data, even with just two scenes, make reasonable, that we will be able to define and extrapolate more comprehensive ice classes from the ALS data under the inclusion of free board heights, in addition to surface roughness, with the final science release of the ALS data. These classes are expected to benefit a lot more from the inclusion of contextual data in our model, than the pure estimation of surface roughness does. It is clear that the matching of products is good enough to extract meaningful data. Classified scenes such as (Fig. 7) inspire confidence, that autonomous ice classification from SAR trained with ALS data will perform competitively and be able relate physical properties of sea ice to SAR imagery consistently.

8. REFERENCES

[1] A. V. Bogdanov, S. Sandven, O. M. Johannessen, V. Y. Alexandrov, and L. P. Bobylev, "Multisensor approach to automated classification of sea ice image data," *IEEE Transactions on Geoscience and Remote Sensing*, vol. 43, no. 7, pp. 1648–1664, 2005.

[2] R. Ressel, A. Frost, and S. Lehner, "A neural network-based classification for sea ice types on X-Band SAR images," *IEEE Journal of Selected Topics in Applied Earth Observations and Remote Sensing*, vol. 8, no. 7, pp. 3672–3680, 2015.

[3] M.-A.N. Moen, S.N. Anfinsen, A.P. Doulgeris, A.H.H. Renner, and S. Gerland, "Assessing polarimetric SAR sea-ice classifications using consecutive day images," *Annals of Glaciology*, vol. 56, no. 69, pp. 285–294, 2015.

[4] N. T. Kurtz, T. Markus, D. J. Cavalieri, W. Krabill, J. G. Sonntag, and J. Miller, "Comparison of ICESat data with airborne Laser altimeter measurements Over Arctic sea ice," *IEEE Transactions on Geoscience and Remote Sensing*, vol. 46, no. 7, pp. 1913–1924, 2008.

[5] S. Singha, M. Johansson, N. Hughes, S.M. Hvidegaards, and H. Skourup, "Arctic sea ice characterization using spaceborne fully polarimetric L-, C-, and X-band SAR with validation by airborne measurements," *IEE Transactions on Geoscience and Remote Sensing*, vol. 56, pp. 3715–3734, July 2018.

[6] Justin F. Beckers, Angelika H.H. Renner, Gunnar Spreen, Sebastian Gerland, and Christian Haas, "Sea-ice surface roughness estimates from airborne laser scanner and laser altimeter observations in Fram Strait and north of Svalbard," *Annals of Glaciology*, vol. 56, no. 69, pp. 235–244, 2015.

[7] T. Geldsetzer and J. J. Yackel, "Sea ice type and open water discrimination using dual co-polarized c-band sar," *Canadian Journal of Remote Sensing*, vol. 35, no. 1, pp. 73–84, 2009.